Extraordinary Infrared Transmission of a Stack of Two Metal Micromeshes

Shannon Teeters-Kennedy, Shaun M. Williams, Kenneth R. Rodriguez, Katherine Cilwa, Daniel Meleason, Alexandra Sudnitsyn, Frank Hrovat, and James V. Coe*

Department of Chemistry, The Ohio State University, 100 West 18th Avenue, Columbus, Ohio 43210-1173

Received: June 15, 2006; In Final Form: September 28, 2006

Two Ni microarrays, stacked in registry with zero open area through the assembly and a subwavelength spacing between the mesh, exhibit transmission resonances through the mid-infrared region that are similar to those of a single mesh. Propagating surface plasmons are coupled between the meshes with this arrangement producing narrower resonances that are isolated from direct transmission. The dispersion behavior of the transmission resonances is well-modeled by propagating surface plasmons if allowances are made for a splitting of the surface plasmon dispersion curve in momentum space because of the coupling of the front and back surfaces of each mesh and perhaps between the meshes. These techniques will be useful for passing infrared radiation through nanospaces enclosed within the mesh stack.

Introduction

Biperiodic metal nanoarrays of subwavelength apertures were first shown by Ebbesen et al. and Ghaemi et al.[1,2] to transmit more visible light than is incident upon their apertures, that is, light initially incident upon optically thick metal is still transmitted without scattering from the incident beam. Ebbesen's extraordinary transmission effect has been moved into the IR region[3−5] using hole-to-hole spacings of ∼10 μm to overlap with the fundamental range of molecular vibrations. Enhanced IR absorption spectra have been recorded using this phenomenon on metal microarrays for self-assembled monolayers,[4−6] adsorbed intermediates of surface-catalyzed reactions,[7] and phospholipids bilayers,[4] including the use of stacked meshes.[4] The extraordinary transmission is generally described as being mediated[1,2,8−10] by surface plasmons (SPs) which are coherent oscillations of the metal's conducting electrons at the surface of the metal. The periodic structure of the mesh interacts with the incident light to produce SPs[11] that propagate along both surfaces of the mesh (coupled through the holes) to another hole where they emerge as photons having the same direction as the incident beam (as pictured in part A of Figure 1). The fundamental nature of the single-mesh phenomena has been established by a variety of studies including ultrafast behavior,[12] entangled photons,[13] polarization effects,[14] SP propagation between separated subwavelength arrays,[15] and dispersion studies.[14,16] These studies indicate a single-photon process[13] that can preserve phase[12] and polarization,[17] at least under some conditions.

Ebbesen's extraordinary transmission effect is characterized by the observed transmittance relative to the fractional open area of the mesh. Enhancement factors of 3−5 in the IR with a single mesh have been reported by us and values as large as 7 have been reported by others.[18] Such observations indicate that transmission is dominated by light that initially hits optically thick metal, that is, a significant path length perpendicular to the incident beam is obtained along the metal front or back surface without scattering from the incident beam. A geometry has been configured, as shown schematically in part C of Figure 1 and with a scanning electron microscope (SEM) image in part D of Figure 1, that permits no transmission directly through the assembly. When this assembly is placed in the sample region of a standard Fourier transform IR spectrometer (FTIR), the principle result is obtained: ∼4% of the beam is still transmitted to the spectrometer's detector. By the above mentioned, single-mesh criteria, any observed transmission divided by the fractional open area of zero corresponds to an infinite value for the enhancement factor. In addition to an "infinite" transmission enhancement, the double-stack configuration produces narrower resonances and eliminates direct transmission which dilutes the SP-mediated transmission of single-mesh experiments.

The coupling between the two meshes in a stack can, in general, have signatures similar to the coupling between the front and back surfaces of a single mesh, so attention is devoted to both mesh−mesh and front−back coupling effects. The front and back surfaces of a single-metal microarray are coupled through the holes producing a splitting of the transmission resonances into symmetric and asymmetric features (see Figure 2). A later section examines and justifies this observation by comparison to experimental infrared attenuated total reflection (ATR) work[19−21] and theory due to Economou[22] to determine if there are any changes upon stacking. The current double stacks of mesh are close, perhaps touching in places, and otherwise have a spacing that is a small fraction of the wavelength. No waveguide modes or splittings are expected[11,23] on the basis of ATR work with such a spacing. Our stacked results are dominated by the front−back coupling of single pieces of mesh, but there may be a small increase in this splitting because of mesh−mesh coupling.

Dispersion studies (in this case, the change in the position of transmission resonances as the mesh is rotated relative to the incoming beam of the spectrometer) are important in assessing the role of SPs. Transmission of the two mesh stack has been studied with both s- and p-polarized incident light to elucidate and verify the propagating SP nature of the transmission resonances. Not all of the single-mesh transmission is attributable to propagating SPs (see Figure 1 in our work about methanol on copper oxide coated mesh[7]) and some still argue with any contribution of SPs.[18] These data are analyzed to obtain dispersion curves for comparison to the known behavior of propagating SPs with particular attention to front−back cou-

* Author to whom correspondence should be addressed. E-mail: coe.1@osu.edu.

10.1021/jp063745l CCC: $37.00
Published on Web 12/06/2006

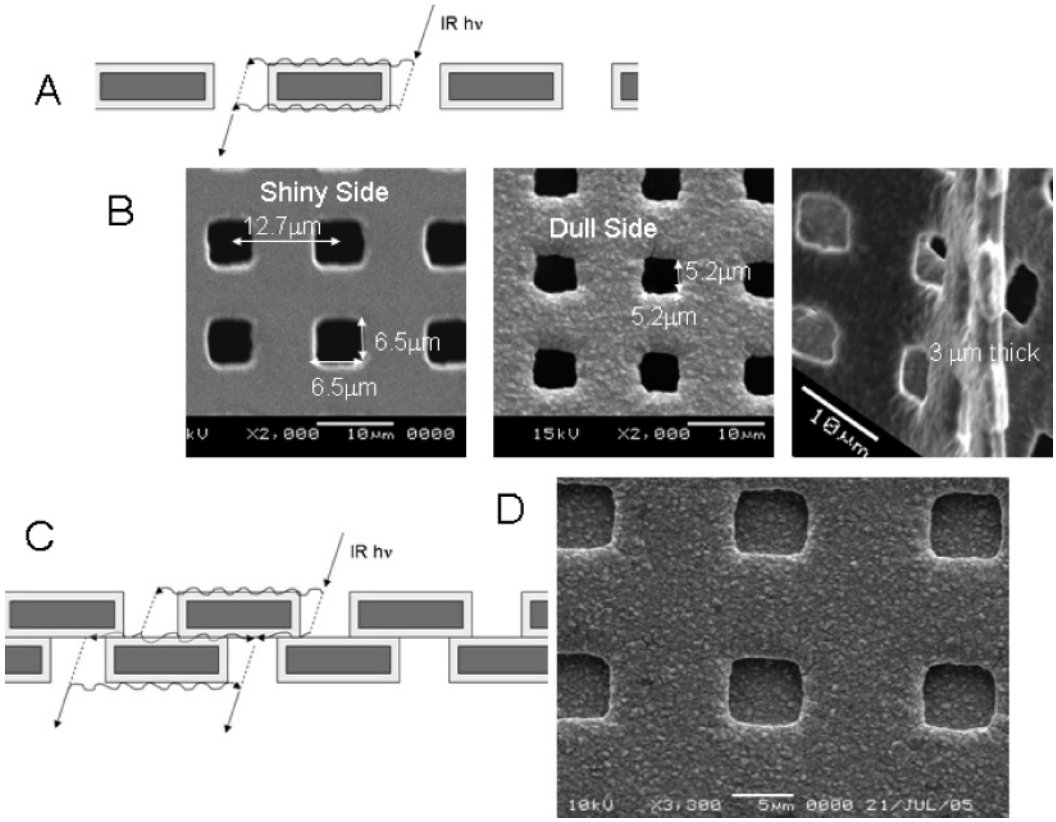

Figure 1. Schematics of the surface-plasmon-mediated extraordinary transmission effect with one mesh (A) and a stack of two (C). Scanning electron microscope images of the front, back, and side of a single Ni mesh (B) and of a stack of two such meshes (D) aligned so no light can proceed straight through the assembly. A considerable portion of the beam from an FTIR spectrometer passes through the stacked assembly (D) without compromising the spectrometer's operation which enables IR absorption spectra to be recorded of nanocoatings on the Ni mesh.

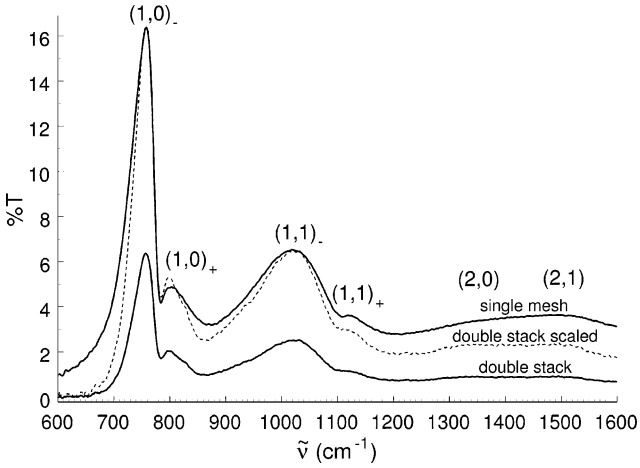

Figure 2. Zero-order FTIR transmission spectra at perpendicular incidence of a single piece of Ni mesh (top solid trace) and a double stack of the same mesh in registry (lower solid trace). The double-stack trace is scaled (dotted trace) to the single-mesh intensity at the $(1,0)_-$ resonance. The two most intense transmission resonances are split because of front−back SP coupling. They are labeled with "+" or "−" subscripts for symmetric or antisymmetric. The symmetric ones are much less intense. Both spectra are very similar except that the double stack has narrower resonances which are less diluted by the broad direct transmission background.

pling, mesh−mesh coupling, and the s-polarized behavior of propagating SPs on bigrating structures (SPs on one-dimensional gratings are a purely p-polarized phenomena). The splitting of the data at perpendicular incidence presents a simple method to determine the SP dispersion curve which is compared to that determined with a full, angle-scanned dispersion analysis.

Mesh and Mesh Stack Details. The finest commercially available metal mesh (made by Precision Eforming, 839 Route 13 Cortland, NY 13045) was used to move Ebbesen's extraordinary optical transmission effect into the infrared (part B of Figure 1). The mesh comes in 15 cm × 15 cm sheets and is currently available only in Ni. The mesh holes are arranged as a square lattice with a hole-to-hole spacing (L) of nominally 12.7 μm and a thickness (h) of ∼3 μm. The holes are primarily square in cross section, though the corners are rounded. The specifications vary a bit from batch to batch. They typically have a width (a) of about 5.5−6.5 μm on the smooth side tapering to ∼4.5−5.0 μm toward the rougher side of the mesh. Unpolarized, zero-order transmission spectra of a single piece of this mesh have been reported previously.[5,16] Several preliminary studies[4,5] have been reported showing that if two such meshes are stretched and stacked upon each other, they still exhibit Ebbesen's extraordinary transmission effect. In fact, a four-mesh stack[4] has been made which still transmitted 22% of the incident beam of an FTIR spectrometer.

In this experiment, a single 8 mm by 5 mm piece of mesh was stretched and secured over a 3.1-mm diameter stainless steel aperture and was placed over a diffuse source of light. A second piece was loosely secured with tape at one edge over the first piece of mesh and was roughly aligned. A gridded interference pattern was observed that displayed a larger spacing between elements as the meshes were better aligned. The upper piece was manipulated for better alignment until the grid pattern was bigger than the size of the mesh. At this point, small manipulations would change the system from dark to light depending on whether the holes were overlapping or not.

Extraordinary IR Transmission of Single Mesh and Double Stack at Perpendicular Incidence. The zero-order transmission spectra of a single piece of mesh and an aligned double stack including the single piece are compared in Figure 2. The double stack shows the same resonances as seen with a single piece of mesh but with less direct transmission (a broad background), narrower resonances, and less intensity. The resonances are labeled by $(|i|,|j|)_\pm$ (see Figure 2) where i and j are steps along the reciprocal lattice (they also label diffraction spots that are no longer transmitted at sufficiently long wavelengths, instead giving rise to SPs[4,24]) and the subscript indicates whether the coupled resonance is the symmetric (+) or asymmetric (-). The pairs of resonances present a spectral signature for the coupling, and in this case, the symmetric features are much weaker. The transmission resonances are observed at wavenumbers given by

$$\tilde{\nu}_\pm = \frac{\sqrt{i^2+j^2}}{Ln'_{\mathrm{eff},\pm}} \tag{1}$$

where L is the hole-to-hole spacing of the square lattice microarray, i and j identify the resonance, and n'_{eff} is the real part of the index of refraction. The parameter, n'_{eff}, determines the shape of the corresponding SP dispersion curve in momentum space and is not necessarily a constant with wavelength. The parameter, $n'_{\mathrm{eff},+}$, is ~1.000 in the mid-IR with most air/metal interfaces as determined by $\mathrm{Re}\{\sqrt{\epsilon_m/(\epsilon_m+1)}\}$[11] where ϵ_m is the complex dielectric of the metal. The parameter, $n'_{\mathrm{eff},-}$, varies with the strength of the front−back coupling (from 1.0 to ~1.1 in the mid-IR with our meshes). The maxima, $\tilde{\nu}_\pm$, of the single mesh $(1,0)_-$, $(1,0)_+$, $(1,1)_-$, and $(1,1)_+$ resonances occur at 758.1, 803.6, 1018.8, and 1118.7 cm^{-1}, respectively. The change in the effective index of refraction because of front−back coupling is given by

$$n'_{\mathrm{eff},-} - n'_{\mathrm{eff},+} = \frac{1}{L}\left(\frac{1}{\tilde{\nu}_-} - \frac{1}{\tilde{\nu}_+}\right) \tag{2}$$

taking n_{eff} values as constant between the pair of resonances. The (1,0) resonance gives $n'_{\mathrm{eff},-} - n'_{\mathrm{eff},+} = 0.059$ at 781 cm^{-1} (average of coupled pair), while the (1,1) resonance gives $n'_{\mathrm{eff},-} - n'_{\mathrm{eff},+} = 0.069$ at 1069 cm^{-1}. If $n'_{\mathrm{eff},+} = 1.000$, that is, in the absence of metal oxides, then $n'_{\mathrm{eff},-}$ would be 1.059 at 781 cm^{-1} and 1.069 at 1069 cm^{-1}. A full, angle-varied, dispersion study (projecting observed resonances by the grating coupling outside the light line) of a similar single Ni microarray assumed that $n'_{\mathrm{eff},-}$ was constant[16] versus wavelength giving $n'_{\mathrm{eff},-} = 1.061$ which is in very good agreement with this simpler procedure. Since the resonances occurring at different frequencies give different $n'_{\mathrm{eff},-}$ values, one might assume a linear dependence with wavenumber, $n'_{\mathrm{eff},-} = b + m\tilde{\nu}$. In this case, the two resonances give two equations with two unknowns yielding $b = 1.032$ and $m = 3.47 \times 10^{-5}$ cm. The corresponding SP dispersion curve is

$$\tilde{\nu}_-(k_{||}) = \frac{-b + \sqrt{b^2 + 4m\left(\frac{k_{||}}{2\pi}\right)}}{2m} \tag{3}$$

which expands in $k_{||}$ as

$$\tilde{\nu}_-(k_{||}) = \frac{1}{2\pi b}k_{||} - \frac{m}{4\pi^2 b^3}k_{||}^2 + O(k_{||}^3) \tag{4}$$

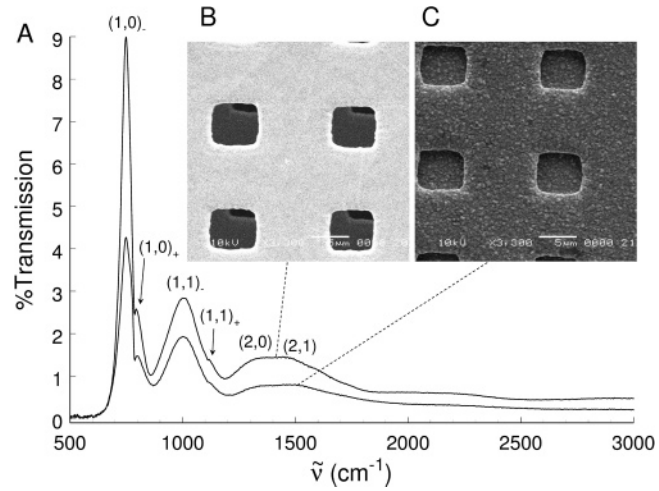

Figure 3. Zero-order FTIR transmission spectra (A) of two different Ni mesh stacks showing transmission resonances (perpendicular incidence, 100 scans, 4 cm^{-1} resolution, DTGS detector, Perkin-Elmer Spectrum GX). The top trace goes with the top left SEM (B) which has an open area of 1.4% and a transmission of 9% (at 748 cm^{-1}) corresponding to a transmission enhancement factor of 6.4. The bottom trace goes with the SEM on the top right (C) for a stacked system with no open area which remarkably still transmits 4.3%, a workable amount of light. The transmittance relative to fractional open area is infinite.

The SP dispersion curve is dominated by a linear term with increased downward bending at higher momentum wavevectors, as has been observed for front−back coupling in other systems.[11,22,25−27]

Several aligned double stacks were constructed for more detailed studies as presented in Figure 3. SEM images (parts B and C of Figure 3) reveal stacks in registry where one system has a slight amount of hole overlap (B) and another has almost no overlap of holes (C). The assembly shown in part B of Figure 3 shows 1.4% open area and the corresponding IR transmission spectrum at perpendicular incidence (top trace in part A of Figure 3) shows 9% transmission at 748 cm^{-1}. This is an enhancement factor of 6.4 which is close to the largest reported enhancements seen with single-mesh arrays. The bottom trace in part A of Figure 3 is a zero-order FTIR transmission spectrum at perpendicular incidence corresponding to the stack with zero open area (part C of Figure 3). When visible light was shined onto this mesh, no light was detectable at low scattering angles. The transmission of 4.3% at 748 cm^{-1} by a double stack with zero open area represents an infinite enhancement by the criterion of transmittance divided by fractional open area. Basically, a workable amount of light is transmitted without scattering in spite of the lack of straight-through paths. The maxima of the $(1,0)_-$, $(1,0)_+$, $(1,1)_-$, and $(1,1)_+$ resonances of the part C double stack occur at 749.0, 801.7, 1000.4, and 1119.5 cm^{-1}, respectively, and those of the part B stack occur at 748.8, 794.0, 1001.7, and 1116.9 cm^{-1}. This corresponds to $n'_{\mathrm{eff},-} = 1.069$ at 775 cm^{-1} and $n'_{\mathrm{eff},-} = 1.084$ at 1060 cm^{-1} ($b = 1.028$, $m = 5.27 \times 10^{-5}$ cm from eq 3) for the part C double stack and $n'_{\mathrm{eff},-} = 1.060$ at 771 cm^{-1} and $n'_{\mathrm{eff},-} = 1.081$ at 1059 cm^{-1} ($b = 1.004$, $m = 7.30 \times 10^{-5}$ cm) for the part B double stack. Basically, the splittings are similar but slightly larger than those of the single mesh.

Transmission Spectra of Mesh Stack versus Angle. Full dispersion studies serve as a more rigorous test of the SP approach. If the coupled SP dispersion curves determined above are reasonable, then they should do a good job at representing the full dispersion data sets. Taking the z-direction as perpendicular to the mesh stack and with the lattice aligned vertically

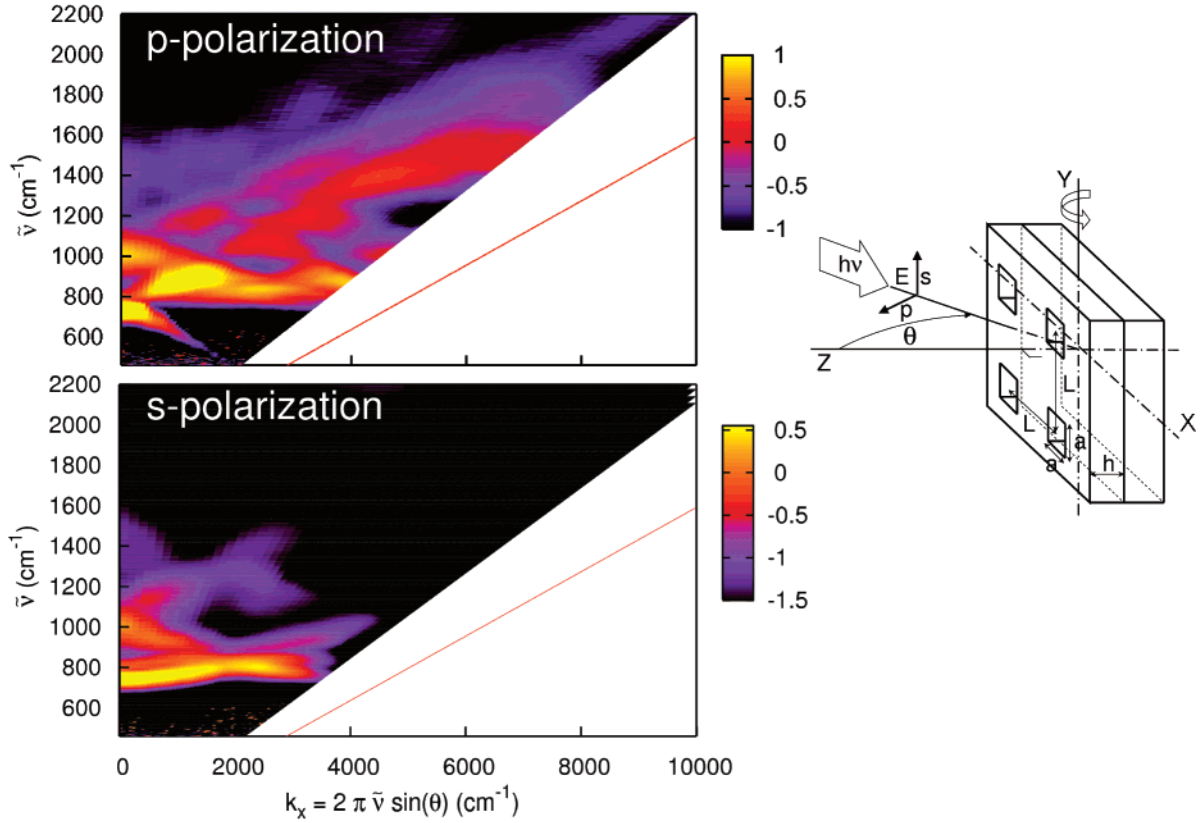

Figure 4. Dispersion plots of the transmission of a two-mesh stack with zero open area. These plots of ln(%T) versus $\tilde{\nu}$ and k_x were created from zero-order FTIR transmission spectra from angles of $\theta = -3$ to 45° in steps of 1° with s- and p-polarization as defined by the schematic on the right (100 scans on a Perkin-Elmer Spectrum GX FTIR, 4 cm^{-1} resolution, DTGS detector, ~16 min for each spectrum, 1/cos(θ) intensity correction). Color indicates transmission on a natural log scale where yellow is max and black is min. The bottom %T trace in Figure 3 corresponds to a vertical cut through these plots at $k_x = 0$; the right edge of the data is 45°, and the red line is the "light line" corresponding to light parallel to the surface, i.e., at $\theta = 90°$.

(y-axis) and horizontally (x-axis, see right side of Figure 4 so that $k_{||} = k_x$), transmission spectra were recorded with linearly polarized radiation (both the s- and p-polarizations) upon rotation from $\theta = -3$ to 45° of the mesh about the y-axis. The momentum wavevector of the photons parallel to the surface was calculated at each point in each spectrum as $k_x = 2\pi\tilde{\nu}\sin(\theta)$ and the transmissions of all 49 spectra are presented with color (yellow is maximum and black is minimum) versus $\tilde{\nu}$ and k_x in Figure 4. The dispersion plots of the double stack (Figure 4) are more structured than their single-mesh counterparts[16] which is likely due to the exclusion of direct transmission and slightly narrower resonances. Since one-dimensional gratings exhibit only p-polarized SP phenomena, it is interesting that the bigrating structure of the microarrays support s-polarized features. In spite of a range of interesting speculations about the nature of the s-polarized features [geometric surface states,[28,29] composite diffracted evanescent waves[18,30]], they are fully accountable with propagating SPs[16] if allowance is made for front−back coupling.

A Closer Look at Grating-Coupled Propagating SP Dispersion Curves. There is no angle from 0 to 90° at which light can excite SPs on a smooth air/metal interface (hence the need[11] for a prism in ATR studies, surface roughness, or a bigrating in these studies). In other words, the propagating SP dispersion curve lies "outside of the light line", that is, to the right of the red line in Figure 4. To more completely characterize the dispersion of the mesh stack transmission resonances, spectra recorded at different incident angles were fit in frequency space to sums of Lorentzian peaks as shown in Figure 5. The Lorentzian peak shapes give a fair, but not perfect,

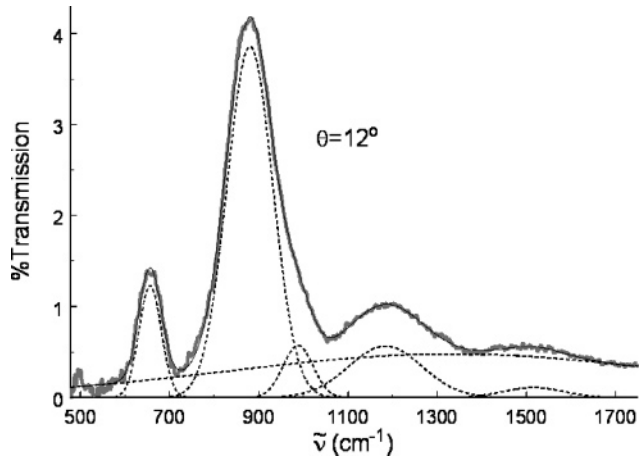

Figure 5. p-Polarized, zero-order transmission spectrum of a two-mesh stack with zero open area (gray solid line) recorded at an incident angle of 12°. This spectrum was fit with a sum of six Lorentzians (black solid line). Each fitted peak is shown with a black dotted line. This fitting procedure was performed on all of the transmission spectra vs wavenumber used to construct the dispersion plots in Figure 4.

representation of the resonance positions. The peak centers extracted from all of the recorded transmission spectra are presented in Figure 6 (p-polarized peaks with filled circles and s-polarized peaks with open circles). The heavier lines at the lower right-hand side of Figure 6 are the SP dispersion curves determined at perpendicular incidence from the resonance positions in Figure 3 for the part C mesh stack. Momentum matching with grating coupling [recalling that $n'_{\mathrm{eff}}(\tilde{\nu}) = b +$

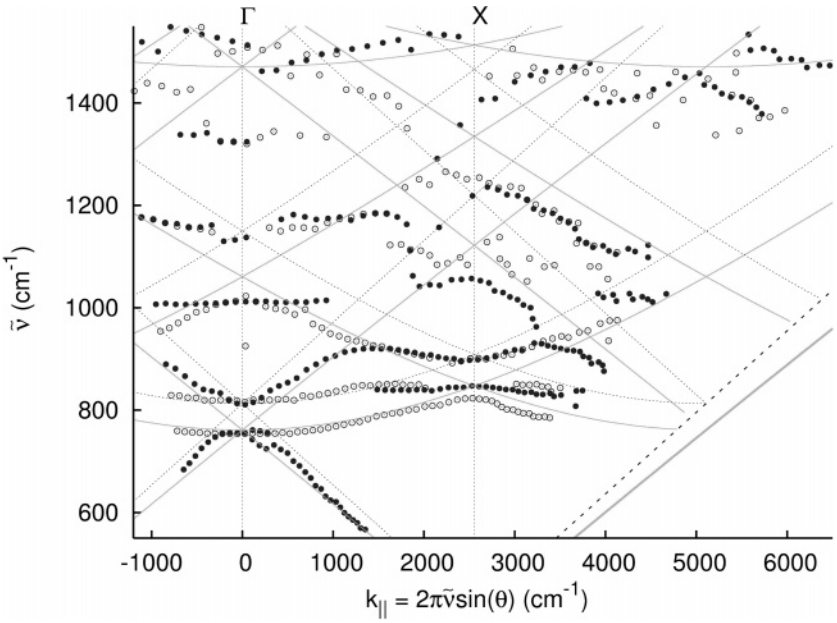

Figure 6. Dispersion diagram of double stack (shown in part C of Figure 3). Peak centers were determined by fitting transmission resonances to Lorentzian lineshapes (as shown in Figure 5). p-Polarized peaks are given with filled circles, while s-polarized peaks are given with open circles. The thicker lines at the lower right-hand side are SP dispersion curves determined with the perpendicular incidence spectra (the lower trace of Figure 3 which gave $b = 1.028$, $m = 5.27 \times 10^{-5}$ cm, $L = 12.3$ μm). The dotted line is the symmetric curve (close to the light line) and the solid line is the asymmetric curve of the coupled pair. Through grating coupling and momentum matching, these lines determine the thinner lines that model the data (dotted for symmetric and solid for asymmetric) inside the light line. The first Brillouin zone (along the nearest hole-to-hole spacing of the square lattice) is represented by the light vertical dotted lines labeled Γ and X.

$m\tilde{\nu}$] yields the asymmetric resonance positions inside the light line as

$$\tilde{\nu}_{(i,j)-}(k_x) = \frac{-b + \sqrt{b^2 + 4m\sqrt{\left(k_x + i\frac{2\pi}{L}\right)^2 + \left(j\frac{2\pi}{L}\right)^2}}}{2m} \tag{5}$$

Similarly, the symmetric resonance positions are given by

$$\tilde{\nu}_{(i,j)+}(k_x) = \sqrt{\left(k_x + i\frac{2\pi}{L}\right)^2 + \left(j\frac{2\pi}{L}\right)^2} \tag{6}$$

The thinner solid lines [asymmetric from eq 5] and dotted lines [symmetric from eq 6] model the data as shown in Figure 6. The lines do a reasonable job of modeling the data at lower frequencies (below 1000 cm^{-1}) justifying the coupled SP approach. The band gaps at about $\tilde{\nu} = 800$ cm^{-1}, $k_{||} = 0$ cm^{-1} and $\tilde{\nu} = 900$ cm^{-1}, $k_{||} = 2500$ cm^{-1} have distinctive patterns characteristic of a bigrating with interesting variations regarding s- and p-polarized sets. While a one-dimensional grating would not show any s-polarized resonances, the s-polarized data of the primary (1,0) resonance shows two curves with an increasing quadratic trend in k_x which is exactly the expectation for propagating SPs[5,16] when the E-field component is not being changed by the angle tuning.

While the perpendicular incidence approach does a reasonable job in the regions of the two resonances that were employed, it seems to lose cohesion in the upper half of Figure 6. Since the data in Figure 6 extend well beyond the first Brillouin zone (indicated with two vertical dotted lines in Figure 6 and labeled Γ and X), all regions were folded back into the first Brillouin zone in Figure 7. These data were simulated by allowing the parameters b and m of eq 5 to vary with attention to the whole dispersion plot yielding simulation parameters of $b = 0.88$, $m = 2.6 \times 10^{-4}$ cm, and $L = 12.3$ μm. These parameters again fit the (1,0) and (1,1) resonances very well, but they also locate

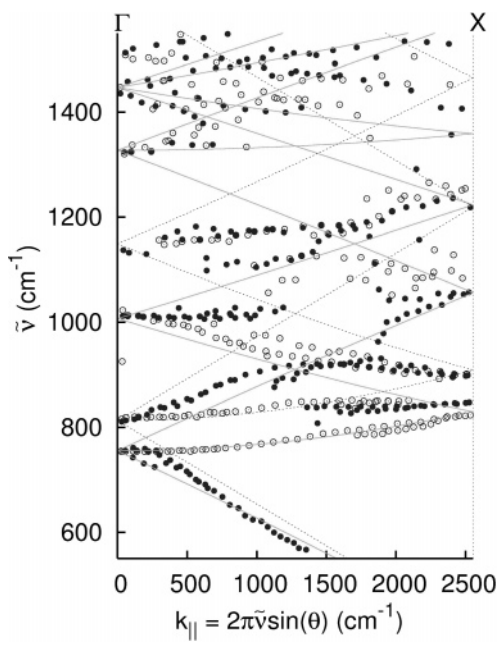

Figure 7. The data in Figure 6 were folded into the first Brillouin zone, and the fitting parameters were changed to better model the data over the whole region. The dotted lines are for the symmetric states and the solid lines are for the asymmetric. These curves correspond to $b = 0.88$, $m = 2.6 \times 10^{-4}$ cm, and $L = 12.3$ μm. These parameters do a better job at modeling the (2,0) and (2,1) resonances.

the positions of the $(2,0)_-$ and $(2,1)_-$ resonances. The new values of b and m (b is smaller and m is larger) yield a larger magnitude for the quadratic term which is proportional to $-m/b^3$ (see the expansion of eq 4) revealing that the asymmetric SP dispersion curve is bending downward more rapidly than expected by the perpendicular incidence approach, that is, the coupling is stronger at higher frequencies and similar to the form predicted by Economou.[22]

Discussion

It is useful to compare the wavelength-scanned, front−back couplings of a single, biperiodic, metal mesh with the interface−interface coupling seen in wavelength-fixed ATR experiments.[11] A laser is reflected off of a thin metallic coating on one side of a prism in ATR experiments. Dips in the reflectivity versus angle of incidence arise because of the excitation of SPs along the air−metal interface. If a second metal film is added to an ATR prism device spaced by a dielectric of thickness on the order of the probing wavelength (Otto geometry), then it is possible to observe a second resonance which is shifted to higher angle and therefore higher momentum. Such resonant angles (θ) can be converted to a momentum wavevector parallel to the metal interface ($k_{||} = 2\pi\tilde{\nu} \sin \theta$) and then to an effective dielectric with $\tilde{\nu} = k_{||}/2\pi n'_{\mathrm{eff}}$. The splittings between these types of resonances were theoretically elucidated by Economou[22] and arise from the coupling of SPs between the two metal/dielectric interfaces. The ω_+ mode is symmetric with in-phase SPs on both interfaces, and the ω_- mode is out-of-phase. One infrared ATR study by Fuzi et al.,[20] with Ni films and an air gap, found two resonances at $\theta_+ = 43.38°$ and $\theta_- = 45.02°$ with $\lambda = 3.391$ μm and a fitted gap of 9.8 μm. Assuming that the ω_+ resonance was on the light line, this corresponds to $n_- = 1.030$. The strongest observed coupling in a more extensive infrared ATR study by Yang et al.,[21] using silver films, $\lambda = 3.391$ μm, and a fitted air gap of 5.3 μm (1.6 wavelengths), gives $n_- = 1.053$. Welford and Sambles[19] have also pursued visible experiments where two silver-coated ATR devices are arranged with a wavelength-scale spacing between the two air/metal interfaces. This device also shows interface−interface SP coupling which is a strong function of air gap spacing. Notably, it exhibits transmission just like our biperiodic mesh systems. Resonance positions were measured equally well in reflectance or transmission. An analysis using $\lambda = 632.8$ nm and an air gap of 764 nm (or 1.21 wavelengths) gives $n_- = 1.050$. All of these results are similar to our recent work on a single piece of Ni mesh[16] ($n_- = 1.061$) and the current mesh results which vary from $n_- = 1.06-1.09$.

Very thin, nonperforated metal films also display[11,19,22,25,31,32] a splitting because of coupling between the two metal/dielectric interfaces. In fact, SP coupling of this sort was characterized earlier with electron beam studies[26,33] at high momentum wavevector values. Intensities of the ω_- and ω_+ modes show differences in experiments with metal between the two interfaces as compared to those with an air gap between dielectric/metal interfaces. The ω_- mode confines more energy between the interfaces,[19] so it is more intense than the ω_+ mode when the region between the interfaces is air rather than metal (which is more absorbing than air). Biperiodic metal mesh has both metal and air in the region between the interfaces, so it was not immediately obvious whether the ω_- or ω_+ mode would be more intense. Experimentally, the mesh's ω_- mode is much more intense suggesting that the system is better modeled by an effective system of two metal films spaced by a dielectric gap rather than a single thin metal film. More quantitative expectations were developed by digitizing results from Yang et al.[21] which were fit by us to give the following relation for n_- as a function of pure air gap thickness

$$n_- = 1.000 + 0.150\left(\frac{t}{\lambda}\right)^{-2.34} \tag{7}$$

where λ is the incident wavelength (3.391 μm in this case) and t is the thickness. As t gets larger, n_- gets closer to n_+ and the coupling gets weaker. Use of this relation with our mesh, where the primary $(1,0)_-$ occurs at 758.1 cm^{-1} or 13.19 μm and $n_- = 1.059$, gives an effective thickness of 20 μm (1.5 wavelengths) even though the mesh is only ~3 μm thick. The metal in-between the two mesh interfaces has the effect of reducing the coupling expected from a 100% air gap of the same size which seems reasonable.

Conclusion

Two Ni meshes stacked in registry have been shown to exhibit an infinite enhancement by the criteria of transmittance divided by fractional open area. From a more practical standpoint, a workable amount of IR radiation is passed through this system with no direct paths. There is great potential for spectroscopic assay of the surfaces of the mesh and the subwavelength space between the mesh. Since there is no direct path through the stack (see Figure 3 part C), clearly all collected photons are traveling in some form, that is, SPs, for distances of many μms in a direction perpendicular to the incident beam before re-emerging as photons.

The stacking of two pieces of mesh in registry shows resonances that are similar to those of a single piece of mesh, except that the resonances are a bit narrower and are not diluted by direct transmission. Detailed dispersion studies show that the SP dispersion curve is split into one curve near the light line and a second curve that is displaced to higher momentum. Since the magnitude of this displacement and the shape of the curve in momentum space of biperiodic mesh are similar to theory[22] and experimental ATR experiments for coupled smooth interfaces,[19,21,34] we conclude that the splittings observed in the biperiodic mesh experiments (both single and double mesh) are dominated by front−back coupling on single pieces of mesh. The double stack of mesh in registry with a small subwavelength spacing shows a small increase in the front−back coupling splitting likely because of mesh−mesh coupling. The observation of splittings because of front−back coupling means that the SPs are traveling on both sides of the mesh.

The stacking of biperiodic mesh is analogous to, but simpler and cheaper than, the placement of two ATR prism devices within a subwavelength spacing.[19] Future work will be directed at defining and varying the spacing between the meshes which could give rise to new resonances, including couplings between the back of the first mesh and the front of the second as well as waveguide modes in the gap between meshes.[19] The mesh transmission resonance widths are largely limited by the time for an SP to get to the next hole, that is, radiation damping from the holes, and this width is about 100 times that of the intrinsic width that is nearly realized in carefully designed ATR experiments.[11] The stacking of mesh poses the possibility that a SP on the first mesh can jump to the second mesh which is rotated so the SP on the second mesh travels much further before finding a hole. Such an arrangement might considerably narrow the resonances and produce longer pathlengths for IR absorption along the surface of the metal. Stacking strategies may prove particularly valuable for probing nanospaces of widths much smaller than the probing radiation. Effective pathlengths sufficient for direct IR absorption add an incisive compliment to existing techniques.

Acknowledgment. We thank the NSF CHE0413077 and ACS PRF 42452-AC5 for support.

References and Notes

(1) Ebbesen, T. W.; Lezec, H. J.; Ghaemi, H. F.; Thio, T.; Wolff, P. A. *Nature (London)* **1998**, *391*, 667.

(2) Ghaemi, H. F.; Thio, T.; Grupp, D. E.; Ebbesen, T. W.; Lezec, H. J. *Phys. Rev. B* **1998**, *58*, 6779.
(3) Moller, K. D.; Farmer, K. R.; Ivanov, D. V. P.; Sternberg, O.; Stewart, K. P.; Lalanne, P. *Infrared Phys. Technol.* **1999**, *40*, 475.
(4) Williams, S. M.; Rodriguez, K. R.; Teeters-Kennedy, S.; Shah, S.; Rogers, T. M.; Stafford, A. D.; Coe, J. V. *Nanotechnology* **2004**, *15*, S495.
(5) Williams, S. M.; Stafford, A. D.; Rodriguez, K. R.; Rogers, T. M.; Coe, J. V. *J. Phys. Chem. B* **2003**, *107*, 11871.
(6) Rodriguez, K. R.; Shah, S.; Williams, S. M.; Teeters-Kennedy, S.; Coe, J. V. *J. Chem. Phys.* **2004**, *121*, 8671.
(7) Williams, S. M.; Rodriguez, K. R.; Teeters-Kennedy, S.; Stafford, A. D.; Bishop, S. R.; Lincoln, U. K.; Coe, J. V. *J. Phys. Chem. B* **2004**, *108*, 11833.
(8) Barnes, W. L.; Dereux, A.; Ebbesen, T. W. *Nature (London*) **2003**, *424*, 824.
(9) Martin-Moreno, L.; Gatcia-Vidal, F. J.; Lezec, H. J.; Pellerin, K. M.; Thio, T.; Pendry, J. B.; Ebbesen, T. W. *Phys. Rev. Lett.* **2001**, *86*, 1114.
(10) Thio, T.; Ghaemi, H. F.; Lezec, H. J.; Wolff, P. A.; Ebbesen, T. W. *J. Opt. Soc. Am. B: Opt. Phys.* **1999**, *16*, 1743.
(11) Raether, H. *Surface plasmons on smooth and rough surfaces and on gratings*; Springer-Verlag: Berlin, 1988.
(12) Dogariu, A.; Thio, T.; Wang, L. J.; Ebbesen, T. W.; Lezec, H. *J. Opt. Lett.* **2001**, *26*, 450.
(13) Altewischer, E.; van Exter, M. P.; Woerdman, J. P. *Nature (London*) **2002**, *418*, 304.
(14) Barnes, W. L.; Murray, W. A.; Dintinger, J.; Devaux, E.; Ebbesen, T. W. *Phys. Rev. Lett.* **2004**, *92*, 107401.
(15) Devaux, E.; Ebbesen, T. W.; Weeber, J.-C.; Dereux, A. *Appl. Phys. Lett.* **2003**, *83*, 4936.
(16) Williams, S. M.; Coe, J. V. *Plasmonics* **2006**, *1*, 87.
(17) Altewischer, E.; Genet, C.; van Exter, M. P.; Woerdman, J. P.; van Zuuk, A.; van der Drift, W. J. M. *Opt. Lett.* **2005**, *30*, 90.
(18) Lezec, H. J.; Thio, T. *Opt. Express* **2004**, *12*, 3269.
(19) Welford, K. R.; Sambles, J. R. *J. Mod. Opt.* **1988**, *35*, 1467.
(20) Fuzi, Y.; Bradberry, G. W.; Sambles, J. R. *J. Mod. Opt.* **1989**, *36*, 1405.
(21) Yang, F.; Bradberry, G. W.; Sambles, J. R. *J. Mod. Opt.* **1990**, *37*, 993.
(22) Economou, E. N. *Phys. Rev.* **1969**, *182*, 539.
(23) Surface plasmon-polaritons. *Proceedings of the Thin Films and Surfaces Group of the Institute of Physics*, London, 1987.
(24) Coe, J. V.; Williams, S. M.; Rodriguez, K. R.; Teeters-Kennedy, S.; Sudnitsyn, A.; Hrovat, F. *Anal. Chem.* **2006**, March 1, 1385.
(25) Kovacs, G. J.; Scott, G. D. *Phys. Rev. B: Solid State* **1977**, *16*, 1297.
(26) Pettit, R. B.; Silcox, J.; Vincent, R. *Phys. Rev. B: Condens. Matter* **1975**, *11*, 3116.
(27) Kloos, T. *Z. Phys.* **1968**, *208*, 77.
(28) Garcia-Vidal, F. J.; Martin-Moreno, L.; Pendry, J. B. *J. Opt. A* **2005**, *7*, *S97*.
(29) Moreno, E.; Martin-Moreno, L.; Garcia-Vidal, F. J. *Los Alamos Nat. Lab. Preprint Archive, Condensed Matter* **2005**, 1.
(30) Gay, G.; Alloschery, O.; Viaris, de Lesegno, B.; O'Dwyer, C.; Weiner, J.; Lezec, H. J. *Nat. Phys.* **2006**, *2*, 262.
(31) Fukui, M.; So, V. C. Y.; Normandin, R. *Phys. Status Solidi B* **1979**, *91*, K61.
(32) Sarid, D. *Phys. Rev. Lett.* **1981**, *47*, 1927.
(33) Schmuser, P. v. *Z. Phys.* **1964**, *180*, 105.
(34) Fuzi, Y.; Bradberry, G. W.; Sambles, J. R. *J. Mod. Opt.* **1989**, *36*, 1405.